Friction Stir Welding of HSLA-65 Steel: Part II. The Influence of Weld Speed and Tool Material on the Residual Stress Distribution and Tool Wear

A. STEUWER, S.J. BARNES, J. ALTENKIRCH, R. JOHNSON, and P.J. WITHERS

A set of single pass full penetration friction stir bead-on-plate and butt welds in HSLA-65 steel were produced using a range of traverse speeds (50 to 500 mm/min) and two tool materials (W-Re and PCBN). Part I described the influence of process and tool parameters on the microstructure in the weld region. This article focuses on the influence of these parameters on residual stress, but the presence of retained austenite evident in the diffraction pattern and X-ray tomographic investigations of tool material depositions are also discussed. The residual stress measurements were made using white beam synchrotron X-ray diffraction (SXRD). The residual stresses are affected by the traverse speed as well as the weld tool material. While the peak residual stress at the tool shoulders remained largely unchanged (approximately equal to the nominal yield stress (450 MPa)) irrespective of weld speed or tool type, for the W-Re welds, the width of the tensile section of the residual stress profile decreased with increasing traverse speed (thus decreasing line energy). The effect of increasing traverse speed on the width of the tensile zone was much less pronounced for the PCBN tool material.

I. INTRODUCTION

As outlined in Part I,[1] there has been considerable interest in the friction stir welding (FSW) process since it was developed by TWI in 1991, in particular for joining aluminum alloys.[2] Although the feasibility of FSW of steel was demonstrated early in the development of the welding process,[3] only recently has there been a significant amount of work published on this subject,[4–9] stimulated by the potential for producing joints with satisfactory mechanical properties and low distortion with applications in the shipbuilding industry.[10] The difficulties associated with developing a low cost tool material that can withstand the high temperatures and forces required for FSW, however, are holding up wider application of the FSW process for ferrous materials.[11,12]

The principles of the FSW technique were discussed in Part I[1] and elsewhere.[2,13] In essence, it is a solid-state joining process whereby a nonconsumable rotating cylindrical tool is plunged into the material at the interface between the plates to be joined and is then moved along the interface. Frictional heat generated primarily from the tool shoulder, and to some extent also from the pin, softens the materials to be joined, which are then plastically deformed around the FSW tool in a constrained extrusion process to combine at the rear of the tool. A high quality solid-state welded joint can be produced, since any surface oxides are broken up and dispersed through local plastic deformation. The fact that the controlling parameters such as tool forces, rotation, and traverse speed can be controlled precisely in an automated FSW process opens up the possibility of making highly reproducible welds. In Part I,[1] the weld microstructure was mapped as a function of weld traverse speed and tool material for HSLA-65 steel friction stir welds. The objective of the present companion study was to examine the residual stress distribution across the same friction stir welds by synchrotron X-ray diffraction (SXRD). The use of this technique also enabled the extent of phase transformation across the weld to be examined. In addition to the SXRD study, laboratory X-ray tomography was carried out on one of the W-Re welds in order to visualize the morphology of tool material deposition in the weld microstructure.

II. EXPERIMENTAL PROCEDURE

A. Materials and Welding Details

Details regarding the FSW trials are given in Part I.[1] HSLA-65 is a high strength, low alloy steel having nominal yield strength of 450 MPa and a relatively high level of toughness due to the low carbon content. The Young's modulus is $E = 200$ GPa and the Poisson's

A. STEUWER is Expert Researcher and Head of User and Industrial Liason with ESS Scandinavia, University of Lund, 22350 Lund, Sweden. S.J. BARNES, NDT Manager, and P.J. WITHERS, Professor of Materials Science, are with the School of Materials, University of Manchester, Manchester M1 7HS, United Kingdom. Contact e-mail: simon.barnes-2@manchester.ac.uk J.ALTENKIRCH, formerly Researcher, School of Materials, University of Manchester, is a Research Associate with the Karlsruhe Institute of Technology. R. JOHNSON, formerly Project Manager, TWI Yorkshire, Catcliffe, Rotherham S60 5TZ, United Kingdom, is retired.

ratio $v = 0.3$. The chemical composition of the HSLA-65 steel plate used in the welding trials is summarized in Table I in Part I.[1] Plates of 6.35-mm (1/4-in.) thickness were joined at TWI (Rotherham, United Kingdom) by friction stir butt welding using a polycrystalline boron nitride (PCBN) tool, while bead-on-plate welds were produced using a W-Re tool. The PCBN tool geometry was a 30 deg tapered pin design with a 20 TPI stepped spiral cut into the surface. The pin was 5.5 mm in length with a 23.7-mm-diameter spiral convex shoulder. The W-Re tool had similar dimensions to the PCBN tool, but had a TRI-FLUTE* pin design with a pin diameter

---

*TRI-FLUTE is a trademark of TWI, Cambridge, UK.

---

of 8 mm at the shoulder and 6 mm at the tip mounted on a 25-mm-diameter concave shoulder. The welding parameters employed for these samples are summarized in Table II in Part I.[1] All of the welds were carried out parallel to the rolling direction of the steel plate. In this article, the notation 400/50 refers to rotation (rev/min)/traverse speed (mm/min).

B. Diffraction Setup for Residual Stress Determination

The measurement of residual strain was undertaken on beam line ID15A at the European Synchrotron Radiation Facility (ESRF, Grenoble, France) using energy-dispersive SXRD. The basic setup is shown in Figure 1, using two solid-state detectors placed at vertical and horizontal scattering angles $2\theta = 5$ deg. The energy range of the white beam is approximately 60 to 250 keV. The general setup and method of data analysis were described in more detail previously.[14] In this configuration, two directions of strain are measured simultaneously: one approximately along the welding direction, defined here as longitudinal, and one
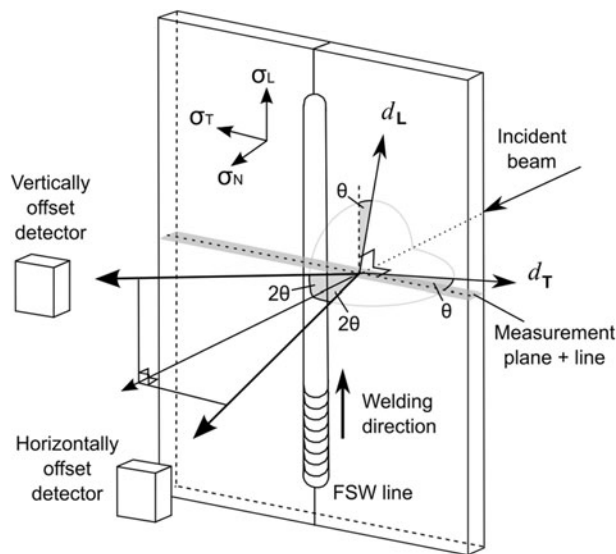

Fig. 1—Experimental setup for nondestructive determination of residual stress on beam line IDI5A. Having two detectors allows for two nearly normal directions of strain to be measured simultaneously.

perpendicular to it, defined here as transverse. The incident beam, as well as the receiving beam, was shaped by slits of 100 μm, which at the given diffraction angles results in an elongated, diamond-shaped gage volume of around 2 mm maximum length. However, most of the diffraction events occur in the central part of the gage volume weighted toward the midthickness of the welded plates. The scan was undertaken midlength, away from the exit/entry points of the FSW tool, in a region that can be assumed to be essentially steady state during welding. The measurement points were spaced 10 mm apart between 110 and 30 mm on either side of the weld line, and 2 mm apart in the weld region within 30 mm of the weld line for the PCBN welds. The corresponding spacings for the W-Re weld measurements were 5 mm apart in the region 75 to 35 mm of the weld line and 2 mm apart within 35 mm of the welds.

The residual stresses were inferred from the measured residual elastic strains, ε, using a biaxial stress model for the longitudinal residual stress σ_L (as shown in Eq. [1]) and likewise for the transverse residual stress σ_T via permutation of the indices:

$$\sigma_L = \frac{E}{1 - v^2}(\varepsilon_L + v\varepsilon_T) \qquad [1]$$

The residual strains $(d - d_0)/d_0$ were calculated assuming a global unstrained lattice spacing, d_0, for both the longitudinal and transverse directions, subjected to stress-balancing conditions in the longitudinal direction and vanishing stresses in the transverse direction at the one plate end.[14,15] There is a possibility that the unstrained lattice spacing d_0 might vary slightly across the weld due to the change in carbon content in the region where there is martensite, but we were unable to detect changes above the uncertainty in lattice parameter measurement.

C. X-Ray Tomography Visualization of Tool Wear Debris

One of the W-Re bead-on-plate weld sections (600/100) was examined using X-ray tomography in an effort to visualize the three-dimensional (3-D) nature of the tool wear traces noted in the weld microstructure in Part I.[1] X-ray tomography was carried out at the Henry Moseley X-ray Imaging Facility, a part of the School of Materials at the University of Manchester, using a Nikon X-Tek system (Nikon X-Tek, Tring, United Kingdom). The system comprises a 225 kV microfocus source (W target) with a 3-μm spot size (boosted to 320 kV), a 5-axis manipulator, and a Perkin Elmer XRD 1621 CT grade 16-bit flat panel detector having 2000×2000 200-μm pixels (Perkin Elmer Optoelectronics, Wiesbaden, Germany). The scan was carried out using a source voltage and current of 245 kV and 60 μA, respectively. 901 radiographs (projections) were collected over 360 deg, with each image being the average of 8 frames of 250 ms exposure. 3-D image reconstruction was carried out using CT Pro software (Nikon X-Tek, Tring, United Kingdom).

III. RESULTS

A. Extent of Phase Transformation

The microstructure and hardness variations across the welds are reported in Part I.[1] This provided evidence that the thermal excursion local to the weld is in excess of the transformation temperature, A_3. Consequently, the as-welded nugget region comprises a mixed martensite, bainite, and proeutectoid ferrite microstructure. The diffraction patterns across the welds showed clear evidence of the presence of traces of austenite (fcc crystal structure) in addition to the phases observed microstructurally, as shown in Figure 2. Figure 2 shows the angular dispersive diffraction pattern. This was obtained from the energy dispersive diffraction pattern as it provides increased flexibility in the peak fitting procedure using the general structure analysis system. The extent of the transformed zone associated with the welding process was estimated using optical microscopy in Part I,[1] but it can also be determined from the extent of retained austenite in the XRD traces. The relatively low intensity of the austenite peaks compared to the ferrite peaks, as well as the fact that the measurements do not satisfy powder averaging conditions, precludes a refinement of their volume fraction using conventional Rietveld techniques. The plot of the {220} austenite peak intensity in Figure 3 as a function of position does allow a qualitative assessment of the lateral extent of transformation as a function of tool type and processing parameters. The amount of retained austenite decreases, as does the extent, with increasing speed ranging from around ±13 mm from the weld line at 50 mm/min to approximately ±11 mm at 250 mm/min traverse speed.

B. Residual Stress Measurements

The experimentally determined longitudinal and transverse residual stresses for both the PCBN and W-Re tool welds are shown in Figures 4 and 5, respectively. Figure 4(a) shows the longitudinal residual stresses for the set of PCBN welds as a function of

Fig. 3—Integrated intensity of the (220) austenite peak (recorded by the vertical detector) as a function of distance from the weld line for the set of PCBN welds.
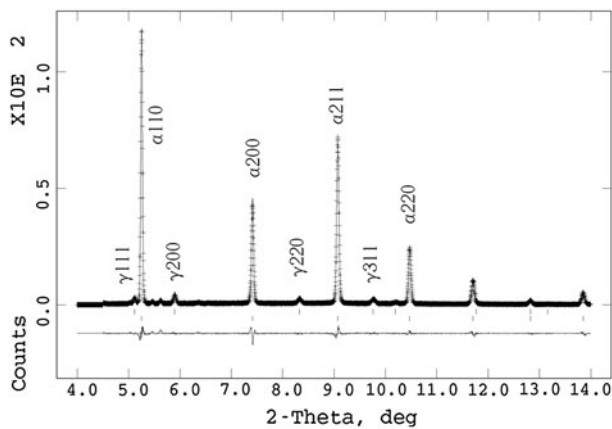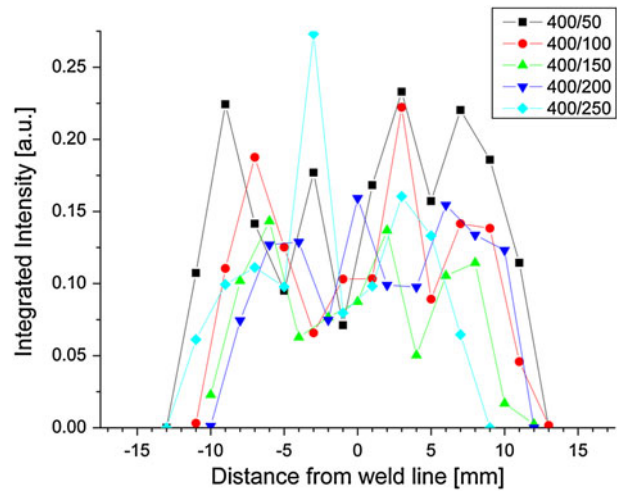
Fig. 2—Fitted diffraction pattern of a 400/50 PCBN weld in the nugget region, showing a mainly ferritic (bcc) structure, with a low level of austenitic (fcc) phase.
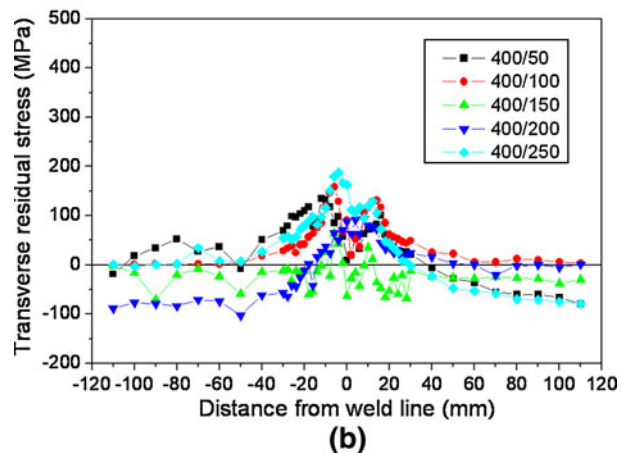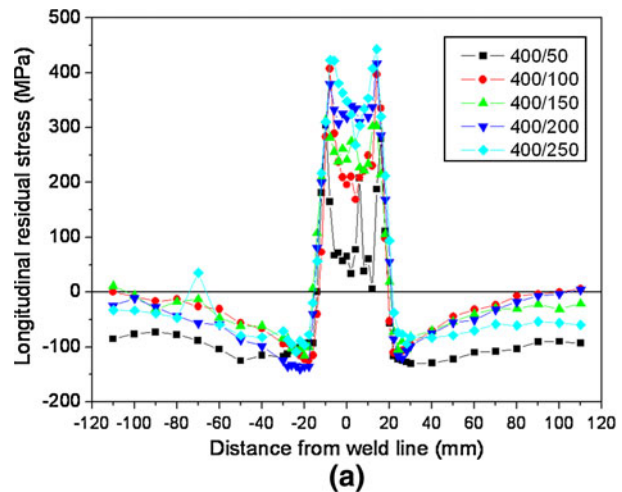
Fig. 4—(a) Longitudinal and (b) transverse residual stresses measured midthickness as a function of distance from the weld line for different traverse speeds for a PCBN tool rotating at 400 rpm. The tool shoulder was 23.7 mm in diameter.
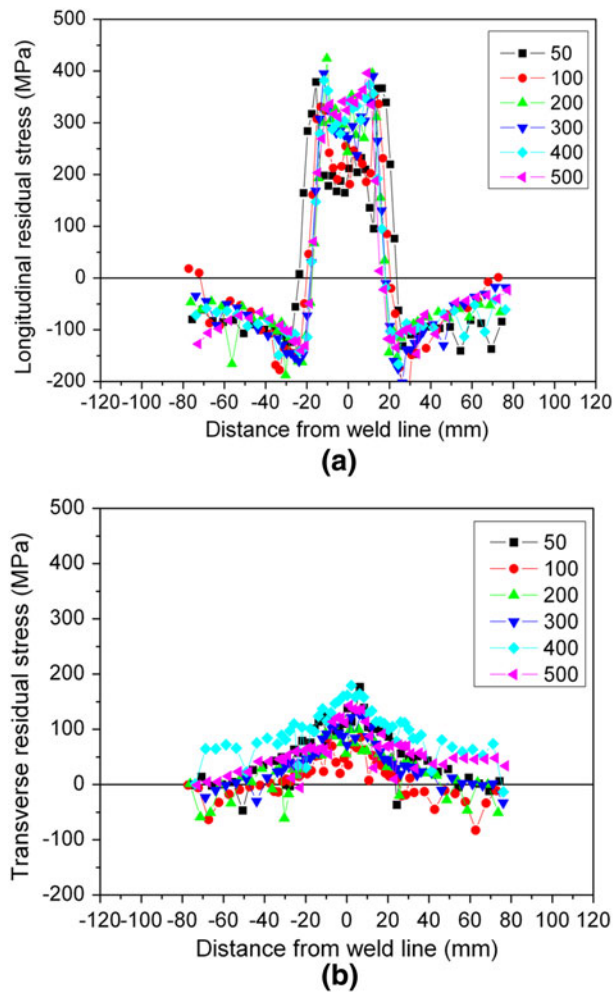
(a)

(b)

Fig. 5—(a) Longitudinal and (b) transverse residual stresses as a function of distance from the weld line for different traverse speeds (mm/min) for a W-Re tool rotating at 600 rpm. The tool shoulder was 25 mm in diameter.

distance from the weld line. The residual stress profile is typical for a normal FSW weld in the sense that high tensile stresses are found just beneath the shoulder approximately 12 mm from the weld line, with a steep transition to balancing compressive stresses in the parent material.[2] In common with many previous FSW experiments,[16,17] the peak tensile stresses are found just beyond the shoulder of the weld tool. While the peak tensile residual stresses are in the region of 400 MPa in all cases (compared to a nominal yield stress of ~450 MPa), the largest residual stresses were observed for the higher traverse speed welds. In the weld stir zone (*i.e.*, at the weld centerline), there is a dip in stress of 50 MPa for the fastest traverse speed, increasing to around 300 MPa for the slowest traverse speed in the PCBN welds. The width of the tensile regions of the residual stress profile appears to be fairly insensitive to the traverse speed, such that the maximum compressive stress is of the order of 100 to 150 MPa and located around 20 mm from the weld centerline in all cases.

The transverse residual stresses for the set of PCBN welds as a function of distance from the weld line are shown in Figure 4(b). These are significantly lower than the longitudinal residual stresses and vary only slightly with traverse speed. There is a slight variation (±50 MPa) in the far-field stress level from sample to sample and from side to side of the butt-welded plates; this may reflect small variations in the stress free lattice parameter arising from small compositional variations from plate to plate.

The longitudinal residual stresses for the corresponding set of W-Re welds are shown in Figure 5(a) as a function of distance from the weld line. The profiles are broadly similar to those shown in Figure 4(a) for the PCBN welds, both in terms of shape and stress magnitudes, although the dip in tensile stress at the weld centerline is less marked, particularly for the lowest traverse speed. In contrast to the PCBN welds, it is also noticeable that with lower traverse speeds, the width of the tensile region becomes broader. As for the PCBN welds, the transverse stresses shown in Figure 5(b) appear to be relatively insensitive to traverse speed, being around 150 MPa in all cases.

The stress near the center of the nugget (averaged within 3 mm of the weld centerline) is shown in Figure 6 as a function of (a) traverse speed and (b) line energy for both sets of welds. A comparison of the effect of traverse speed on residual stress (Figure 6(a)) for the two different tool materials cannot be carried out directly since different rotation speeds were used. The line energy calculation, however, takes into account the tool rotation speed and thus allows a comparison of the tool materials (Figure 6(b)). The tensile residual stresses are slightly higher for the PCBN welds at low line energy values (200 to 250 mm/min traverse speeds). The results for both tool types are similar at medium line energy values (100 to 150 mm/min traverse speeds), but at the highest line energies (50 mm/min traverse speed), the tensile residual stresses in the PCBN weld are significantly lower.

C. Tool Wear Debris

As was noted in Part I,[1] tool wear during FSW results in tungsten-rich bands being observed in the weld microstructure. However, it was difficult to visualize the 3-D morphology from optical micrographs. The aim was thus to exploit the high attenuation of tungsten and rhenium to record a 3-D image of the debris by microscale computed X-ray tomography (micro-CT). Figure 7 shows a reconstructed micro-CT image of the 400/100 bead-on-plate weld made using a W-Re tool. The position and distribution of W-Re rich areas can be clearly discerned. The W-Re deposits at the edge of the stir zone, close to the base of the tool and predominantly on the retreating side. As was noted in Part I,[1] W-Re rich bands were more common for the slower speed welds. While both tool force and tool temperature are important in determining tool wear, the current results seem to suggest that higher tool (and weld) temperatures (slower traverse speeds) are more harmful than higher tool forces (as arise at high speeds). Although W-Re tool wear was reported to occur through a combination of chemical reactions and mechanical abrasion,[18] the
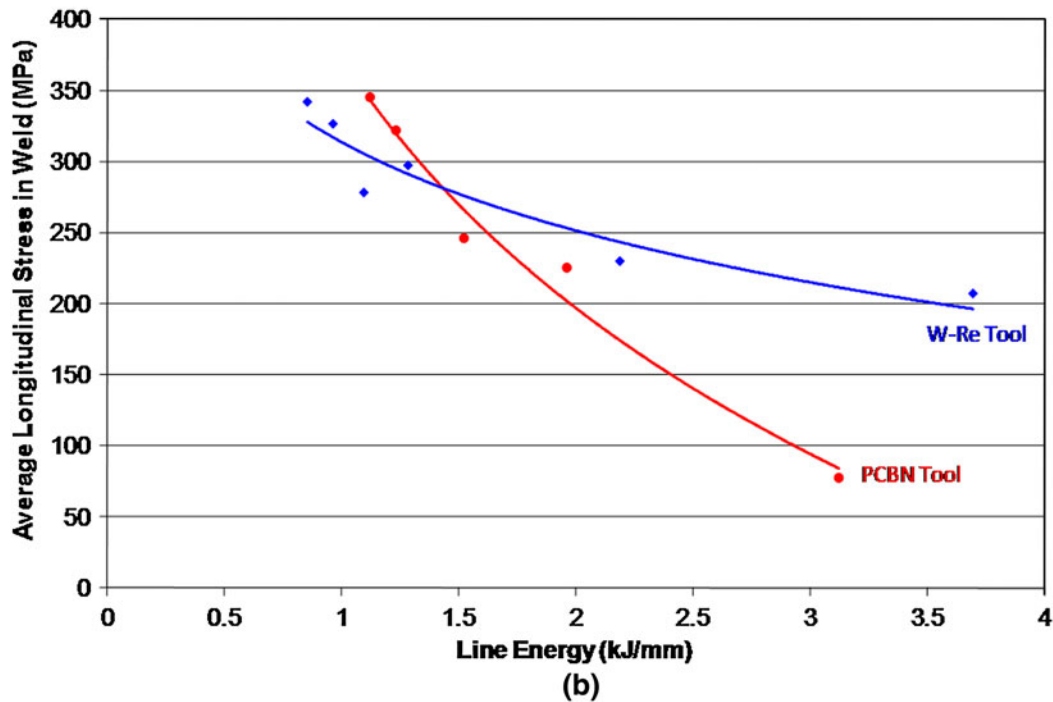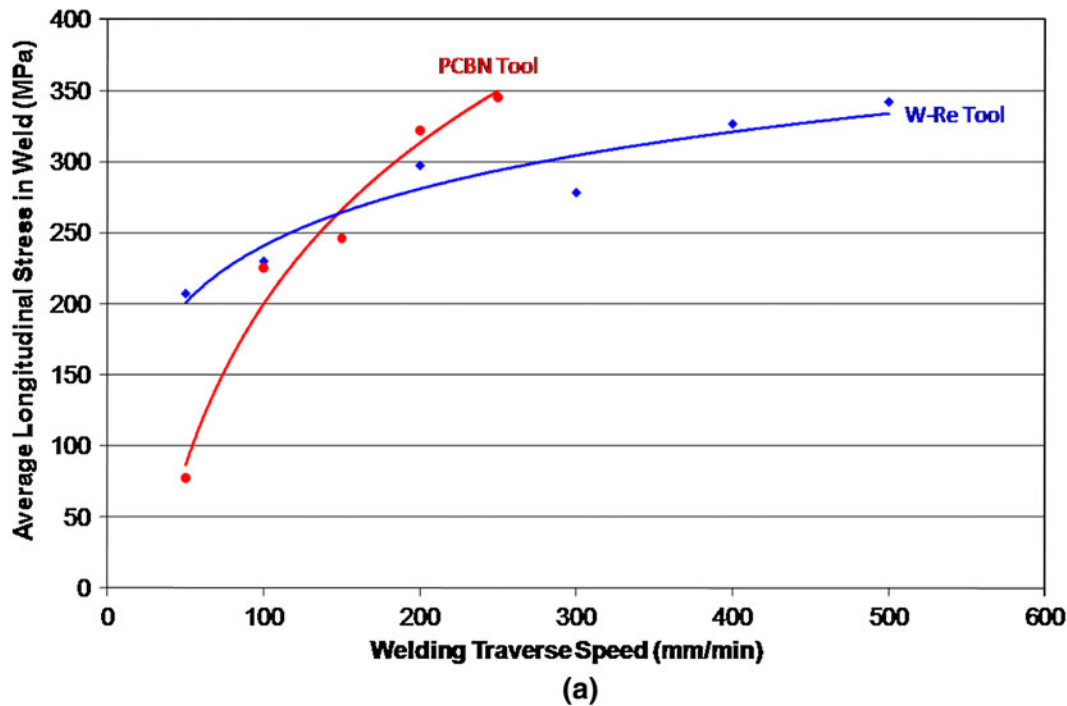
Fig. 6—Average longitudinal residual stress at the midthickness of the weld nugget as a function of (*a*) weld traverse speed and (*b*) line energy for both sets of welds.

current results indicate that there is a greater contribution of chemical wear since tool temperature appears to have the greatest influence. This is in agreement with some previous work[18] and implies that high traverse speeds should be used to minimize W-Re tool wear. The tool wear deposits are mostly seen at the outside diameter of the tool, but not near the tool shoulder even though this is clearly a high-temperature area. As

noted previously,[18] this indicates that there must be a component of the wear that relies on mechanical abrasion, since tool wear is exaggerated in the area of highest rotational velocity.

As reported in Part I,[1] there was no tool debris observed in the PCBN welds. The PCBN tools, however, were much more susceptible to catastrophic failure due to thermal cracking of the tool shoulder. This tends to
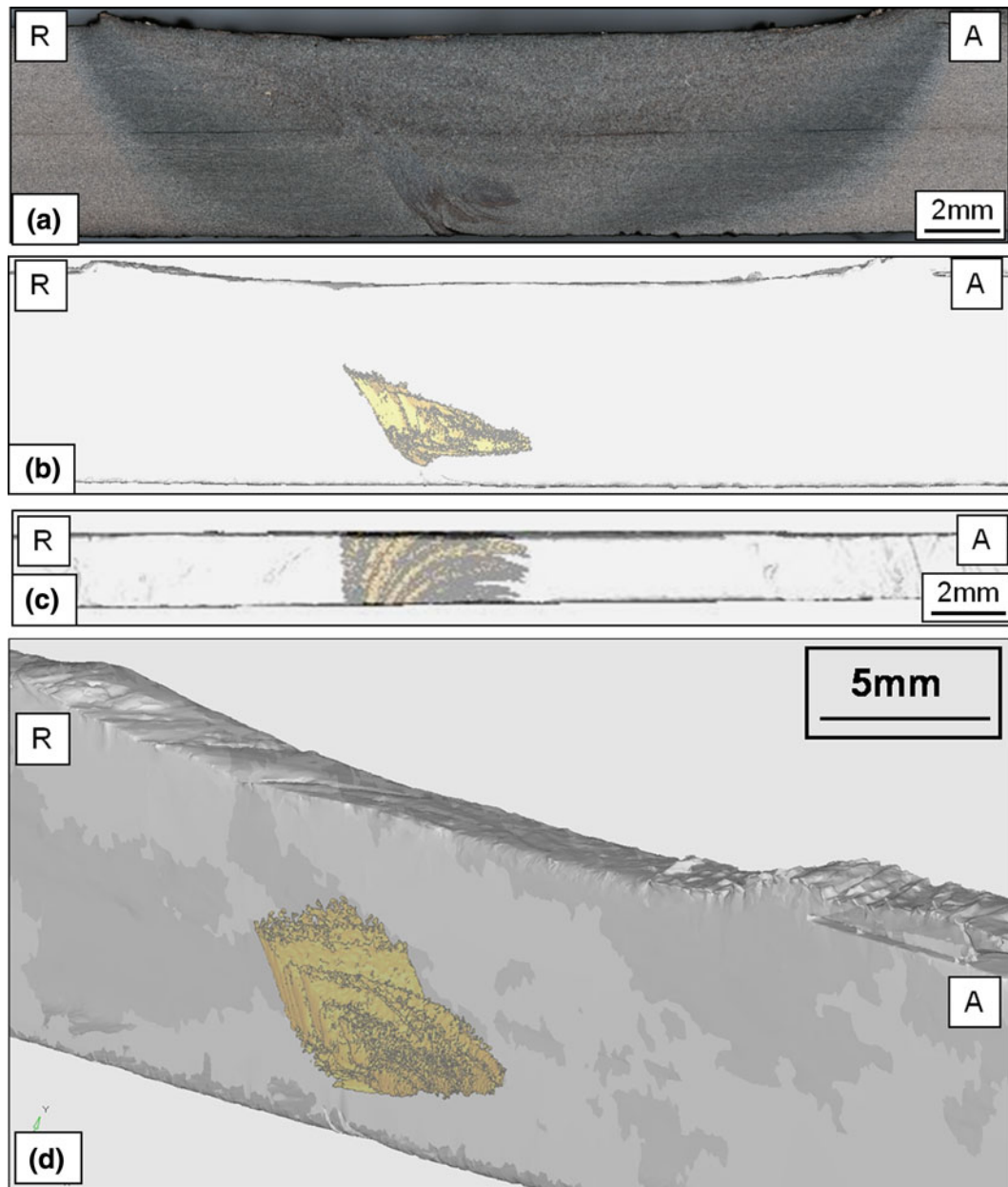
Fig. 7—Comparison of (*a*) the macrostructure of the 100 mm/min W-Re weld with the (*b*) front (*c*) plan view and (*d*) 3-D view from the reconstructed X-ray tomography scan. The yellow area is the higher X-ray absorbtion area associated with W-Re in the weld. The advancing (A) and retreating (R) sides of the weld are indicated.

IV. DISCUSSION

The synchrotron XRD measurements reported here are discussed in light of the microstructure and hardness results already reported in Part I[1] (Figures 8 and 9). The XRD traces indicated the presence of a low level of retained austenite. However, the presence of austenite was not evident from the micrographs presented in Part I,[1] which showed evidence that the stir zone was a mixture of martensite, bainite, and pro-eutectoid ferrite. Nevertheless, it is possible that a small amount of retained austenite is present in the microstructure associated with the martensite in the highest cooling rate/strain rate regions of the weld nugget. Further examination of the microstructure using sodium bisulfite tint etching, however, has not revealed any significant retained austenite in the microstructure.

Figure 8 shows the lateral extent of retained austenite estimated from the XRD results alongside the positions of the edge of the transformed zone and the outer heat-affected zone (OHAZ), determined from the microstructural examination,[1] and the location of maximum

reduce the traverse and rotation speeds that are safely usable with the PCBN tools.
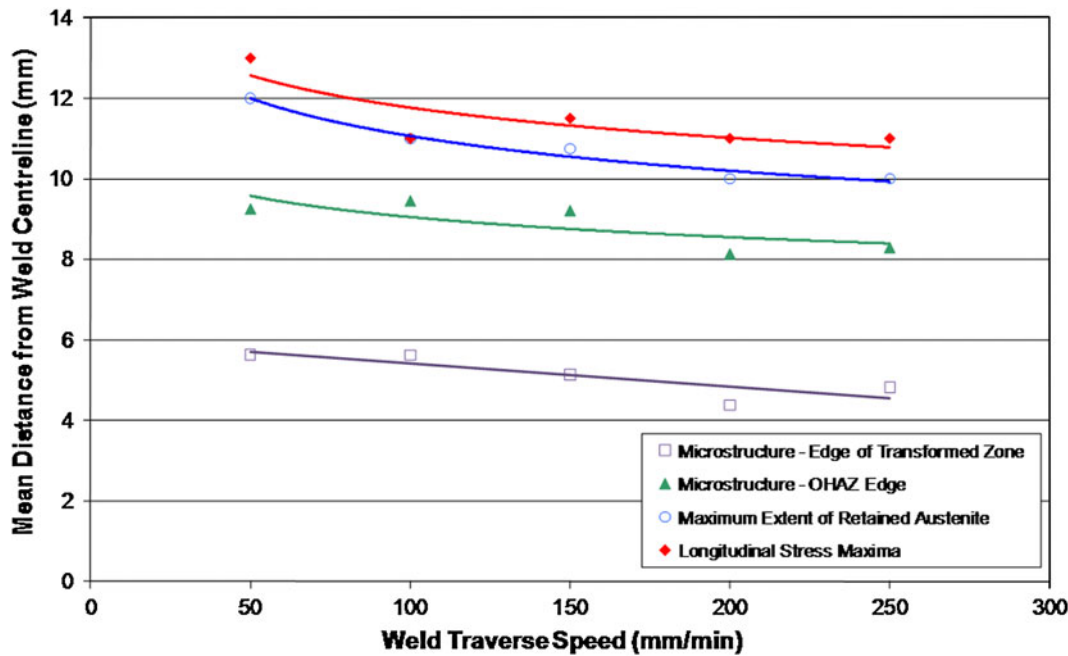
Fig. 8—Effect of weld traverse speed on the position of the maximum longitudinal tensile stress in comparison to the positions of the maximum extent of retained austenite in the microstructure and the outer edge of the transformed zone and OHAZ determined optically for the midthickness of the PDBN welds in Part I.[1]

longitudinal stress. This appears to indicate that retained austenite is present in the microstructure considerably beyond the transformed zone of the weld. This is clearly not physically possible since retained austenite is not generally present in the parent metal. In order to rationalize the synchrotron results, the volume average about the measurement position needs to be taken into account. It is important to remember that although the center of the gage volume for the X-rays is at the midthickness of the weld, the gage volume extends approximately 2.3 mm around the midthickness (plate thickness 6.25 mm). Furthermore, the weld is much broader (±12 mm) near the top than the bottom,[1] and so the width of the OHAZ is greater above the midthickness of the weld. The smearing effect from polishing could be expected to increase the extent of optically measured zones by a further 2 mm on either side. This means that the transformed region measured optically could extend to around 8 mm (for 50 mm/min traverse speed). This is still narrower than the extent of the retained austenite measured by XRD. Once the influence of the gage volume and the measurement interval (every 2 mm from the weld centerline) are taken into account, however, the extent of possible retained austenite is in line with the extent of the OHAZ. This result is more in line with expectations, since a small amount of retained austenite could be present in both the inner heat-affected zone (IHAZ) and middle heat-affected zone (MHAZ) as both these areas were heated above the critical temperature A_1.

Figure 9 compares the location of the maximum longitudinal residual stress with the location of minimum hardness and the edge of the OHAZ as a function of (a) weld traverse speed and (b) line energy. The peak

tensile residual stresses are in the parent metal slightly beyond the extent of the OHAZ and the minimum hardness position. That the maximum residual stress lies in the parent metal just outside the HAZ was noted previously for both friction stir and fusion welding of steel.[4,19] The occurrence of high tensile stresses in this area indicates that this material reached a sufficiently high temperature for large thermal contraction stresses to build during cooling. Unlike the HAZ, the material in the parent metal region is sufficiently strong to maintain much larger tensile contraction stresses during cooling. It is of some concern that the minimum hardness recorded for each weld[1] is associated with the OHAZ due to overtempering, since this region lies just inside the region of maximum tensile stress.

The presence of a dip in the residual stress at the weld line was observed previously in many welding trials, including FSW of aluminum alloys where it is due to the very low strength of the material near the weld line just after the hot tool has passed, causing tensile longitudinal straining of the near weld region as the weld begins to cool.[20] In the current case, the displacive nature of the austenite-martensite/bainite transformation during cooling of the weld nugget acts to reduce the generation of tensile stresses in the nugget. As noted in previous work,[19,21] volume expansion associated with displacive transformations can offset the effect of thermal contraction as the weld nugget cools, or even give rise to compressive residual strains if the transformation occurs at a sufficiently low temperature.[19] In the case of HSLA-65 steel, the transformation completes at a relatively high temperature (1000 K (727 °C)), thus enabling thermal contraction stresses to be generated after the transformation, so that the final load state is
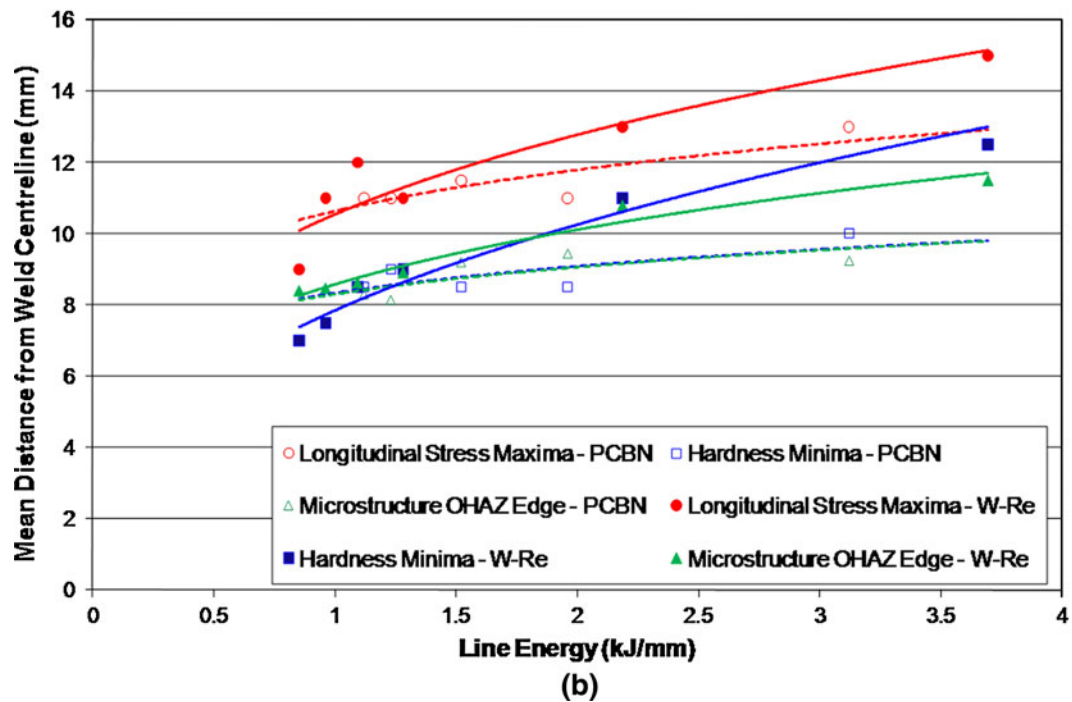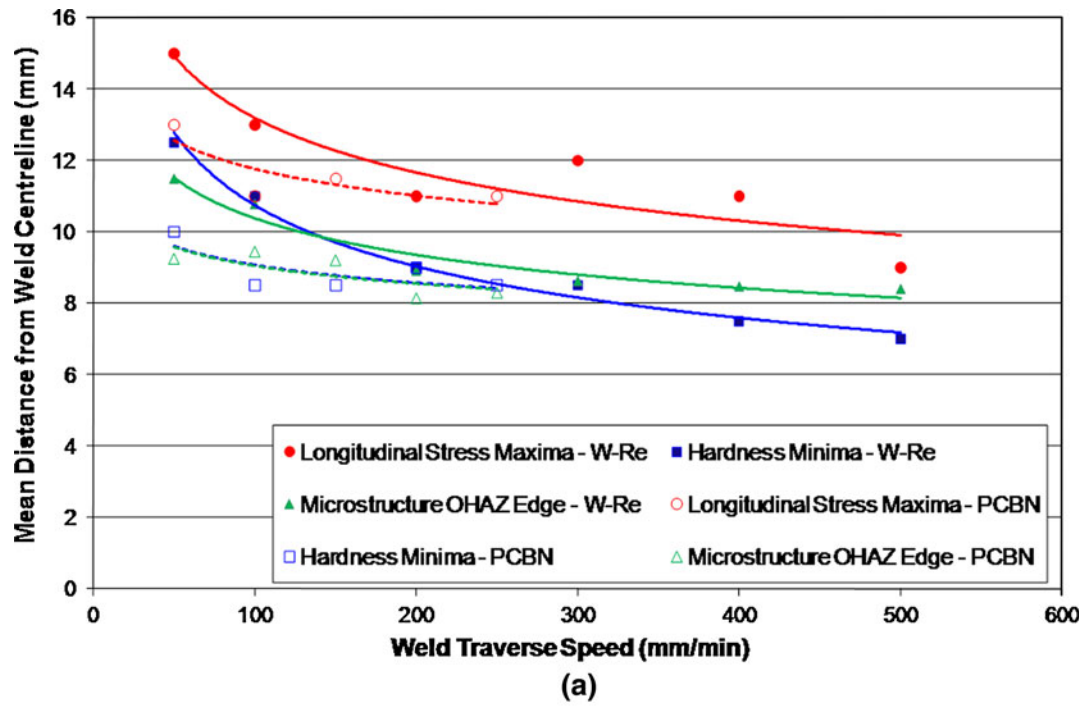
Fig. 9—Effect of (a) weld traverse speed and (b) line energy on the position of the maximum longitudinal tensile stress in comparison to the positions of minimum hardness level and the outer edge of the OHAZ[1] for welds produced with PCBN (dotted line) and W-Re (solid line) tools.

tensile but less than the yield stress. It might be expected that higher extents of displacive transformation (and, therefore, larger dips in tensile stress) would be observed with increasing traverse speed because of the faster cooling rates after the tool has passed, but this is contrary to the current observations. As discussed in Part I,[1] higher traverse speeds also lead to lower peak temperatures, leading to more polygonal ferrite growth and lower extents of martensitic transformation. Consequently, the competing factors of peak temperature attained and cooling rate experienced after the FSW tool has passed determine microstructure, hardness, and residual stress. Both factors are influenced by line energy, tool material, and tool design.

When the residual stress data are compared to the hardness values reported in Part I,[1] the following trends become apparent.

(a) At similar high line energy inputs (low traverse speeds), the weld nugget hardness values are quite similar for PCBN and W-Re welds, but the longitudinal residual stress values are much lower for the PCBN weld.
(b) At similar low line energy inputs (higher traverse speeds 200 to 250 mm/min), the longitudinal residual stress values for the PCBN welds are slightly higher than for W-Re welds. The hardness of the PCBN weld nugget is also somewhat higher than the W-Re weld nugget.

As has already been noted,[1] there are two major influences on the microstructure (and thus hardness) in the weld nugget region: peak temperature attained and cooling rate after the welding tool passes. Both peak temperature and cooling rate are influenced by welding traverse speed (line energy), tool material, and design. As the welding traverse speed increases, the cooling rate after welding also increases, resulting in greater amounts of displacive transformation products in the microstructure and thus higher hardness. The peak temperature reached in the weld nugget, however, is expected to drop with increasing traverse speed. This results in a smaller prior austenite grain size and less martensite on cooling.[1] The effect of faster cooling rate dominates over peak temperature effects to higher traverse speed values in the case of the PCBN welds, leading to higher hardness than the W-Re weld. This is a result of the differences in tool temperature noted previously.[1]

Figure 9 shows that the positions of hardness minima, longitudinal stress maxima, and OHAZ edge sizes are closer to the weld centerline for the PCBN tool. This result is expected on the basis of the line energy comparison when the different thermal properties of the two tool materials are considered. PCBN is a better thermal conductor than W-Re[22] and so would be expected to be more effective in conducting heat away from the weld zone during welding. Samples welded using a PCBN tool, therefore, would be expected to attain lower temperatures than for a W-Re tool with the same line energy input. Additionally, although the line energy calculation takes into account the tool rotation speed, it does not include the effect of coefficient of friction between the steel and the tool material. The PCBN tools are thought to exhibit a lower coefficient of friction than the W-Re tools[23] and thus should generate less frictional heating from a certain line energy input. It was noted previously[1] that the forces used to move the PCBN tool were higher than the W-Re tool for the similar line energy values, particularly at low traverse speeds. This indicates that the PCBN tool is welding at a lower temperature than the W-Re tool. This was confirmed by visual observations during the welding trials.

All other factors being equal, the lower temperature of the PCBN weld should lead to a lower tensile residual stress in the weld nugget than the W-Re weld as is observed for the lowest weld speed. As traverse speeds increase, the greater extent of displacive transformation in the PCBN weld leads to higher hardness. This displacive transformation should lead to lower residual stress in the weld nugget through offsetting the effect of thermal contraction. At the highest traverse speeds for the PCBN welds, however, the tensile residual stress is higher in the weld nugget than for the W-Re weld, possibly as a result of the higher strength weld nugget resisting thermal contraction more effectively.

V. CONCLUSIONS

A number of observations can be drawn from this study.

(a) The maximum residual stresses were located just outside the HAZ of the weld in the parent metal. The maximum stress was similar in both sets of welds being just above 400 MPa, which is close to the nominal yield stress. The weld residual stress profile was very similar to that observed for aluminum alloys despite the presence of displacive transformation products near the weld line.
(b) For the W-Re welds, the width of the tensile section of the residual stress profile decreased with increasing traverse speed (thus decreasing line energy). This was observed in other FSW studies on aluminum alloys.[15,16] The effect of increasing traverse speed on the width of the tensile zone was much less pronounced for the PCBN tool material.
(c) The PCBN tool ran at a lower temperature than the W-Re tool for similar line energy values. This was expected as a result of the lower thermal conductivity and higher coefficient of friction of the W-Re tool. The lower temperature of the PCBN welds resulted in a lower residual stress in the weld nugget at the lowest traverse speed than observed for the W-Re weld. At the highest traverse speeds, the tensile residual stress was slightly higher for the PCBN weld possibly as a result of the stronger weld metal resisting thermal contraction more effectively.
(d) X-ray tomography examination of the W-Re welds showed deposition of W-Re debris in bands mainly on the retreating side of the weld close to the tool tip. Greater deposits were found at the slower traverse speed welds. This indicates that temperature, rather than applied force, is the most significant factor in W-Re tool wear for these welds.

their support in the examination of the W-Re wear traces in the welds. Thanks are also due to Scott Kenningley for his work on the visualization of the W-rich areas in the welds using X-ray tomography.

REFERENCES

1. S.J. Barnes, A.R. Bhatti, A. Steuwer, R. Johnson, J. Altenkirch, and P.J. Withers: unpublished research, 2011.
2. P.L. Threadgill, A.J. Leonard, H.R. Shercliff, and P.J. Withers: *Int. Mater. Rev.*, 2009, vol. 54, pp. 49–93.
3. W.M. Thomas, P.L. Threadgill, and E.D. Nicholas: *Sci. Technol. Weld. Join.*, 1999, vol. 4, pp. 365–72.
4. S.J. Barnes, A. Steuwer, S. Mahawish, R. Johnson, and P.J. Withers: *Mater. Sci. Eng. A*, 2008, vol. 492, pp. 35–44.
5. T.J. Lienert, W.L. Stellwag, B.B. Grimmett, and R.W. Warke: *Weld. J.*, 2003, vol. 82, pp. 1S–9S.
6. A.P. Reynolds, W. Tang, M. Posada, and J. DeLoach: *Sci. Technol. Weld. Join.*, 2003, vol. 8, pp. 455–60.
7. L. Cui, H. Fujii, N. Tsuji, and K. Nogi: *Scripta Metall. Mater.*, 2007, vol. 56, pp. 637–40.
8. H. Fujii, L. Cui, N. Tsuji, M. Maeda, K. Nakata, and K. Nogi: *Mater. Sci. Eng. A-Struct.*, 2006, vol. 429, pp. 50–57.
9. G. Cam: *Int. Mater. Rev.*, 2011, vol. 56, pp. 1–48.
10. T.J. Lienert: *Materials Solutions: Joining of Advanced and Speciality Materials VI*, Pittsburgh, PA, Oct. 2003, pp. 28–34.
11. P.J. Konkol and M.F. Mruczek: *Weld. J.*, 2007, vol. 86, pp. 187S–195S.
12. H.K.D.H. Bhadeshia and T. DebRoy: *Sci. Technol. Weld. Join.*, 2009, vol. 14, pp. 193–96.
13. R. Nandan, T. DebRoy, and H.K.D.H. Bhadeshia: *Progr. Mater. Sci.*, 2008, vol. 53, pp. 980–1023.
14. A. Steuwer, J.R. Santisteban, M. Turski, P.J. Withers, and T. Buslaps: *J. Appl. Crystallogr.*, 2004, vol. 37, pp. 883–89.
15. P.J. Withers, M. Preuss, A. Steuwer, and J.W.L. Pang: *J. Appl. Crystallogr.*, 2007, vol. 40, pp. 891–904.
16. H. Lombard, D.G. Hattingh, A. Steuwer, and M.N. James: *Mater. Sci. Eng. A*, 2009, vol. 501, pp. 119–24.
17. A. Steuwer, M. Peel, and P.J. Withers: *Mater. Sci. Eng.*, 2006, vol. 441, pp. 187–96.
18. J. Bernath, B. Thompson, and N. Ames: *7th Int. Symp. on Friction Stir Welding*, Session 03b, Awaji Island, Japan, 2008, pp. 74–78, TWI, Cambridge, United Kingdom.
19. H. Dai, J.A. Francis, H.J. Stone, H.K.D.H. Bhadeshia, and P.J. Withers: *Metall. Mater. Trans. A*, 2008, vol. 39A, pp. 3070–78.
20. D.G. Richards, P.B. Prangnell, S.W. Williams, and P.J. Withers: *Mater. Sci. Eng.*, 2008, vol. 489, pp. 351–62.
21. W.K.C. Jones and P.J. Alberry: *Ferritic Steels for Fast Reactor Steam Generators*, British Nuclear Engineering Society, London, 1977, pp. 1–4.
22. B.K. Jasthi, W.J. Arbegast, and S.M. Howard: *J. Mater. Eng. Perform.*, 2009, vol. 18, pp. 925–34.
23. C.D. Sorensen and T.W. Nelson: *Friction Stir Welding and Processing*, ASM INTERNATIONAL, Materials Park, OH, 2007, pp. 111–20.